Journal of Organometallic Chemistry, 391 (1990) 377–385
Elsevier Sequoia S.A., Lausanne
JOM 20972

Electron transfer in mixed-valence 1,1,12,12-tetra-n-butyl[1,1]stannaferrocenophane: electrochemical and near-IR spectroscopic studies

Teng-Yuan Dong *, Ming-Yhu Hwang, Yuh-sheng Wen
Institute of Chemistry, Academia Sinica, Taipei (Taiwan)

and Wen-Shu Hwang
Department of Chemistry, National Sun Yat-Sen University, Kaohsiung (Taiwan)

(Received February 1st, 1990)

Abstract

The physical properties of neutral and mixed-valence 1,1,12,12-tetra-n-butyl[1,1]stannaferrocenophanes are reported. The structure of the *endo,endo*-1,12-di-n-butyl-*exo,exo*-1,12-diiodo[1,1]stannaferrocenophane has been determined by X-ray diffraction. The compound crystallizes with monoclinic symmetry, space group $P2_1/C$, a 10.3282(14), b 10.7916(12), c 13.6772(18) Å, β 94.080(12)°, V 1520.57 Å^3, and $Z = 2$. The structure was refined to give conventional discrepancy factors of $R_F = 0.036$ and $R_{WF} = 0.031$. The electron-transfer in the σ-bridged 1,1,12,12-tetra-n-butyl[1,1]stannaferrocenophane cation is attributed to the d–π overlap mechanism of tin atoms and the cyclopentadiene rings.

Introduction

The study of intramolecular electron transfer in mixed-valence complexes should elucidate the factors which affect rates of electron transfer in oxidation–reduction processes, and biological transport chains [1]. In the case of mixed-valence biferrocenium triiodide salts, $[(RC_5H_4)(C_5H_4)Fe]_2I_3$ (R = H [2,3]; ethyl [3,4]; n-propyl [4,5]; n-butyl [3]; and benzyl [3]), the solid-state environment has been shown to play a crucial role in determining the rate of intramolecular electron transfer.

In addition to changing the solid-state environment to probe the factors affecting electron transfer, the architecture of bridged ferrocenes are particularly attractive owing to their variability in structure. To date, only two basic types of bridged mixed-valence biferrocenes have been noted. There are those that have been found to have localized electronic structures. The monooxidized cations of compounds **5**, **6**

0022-328X/90/$03.50

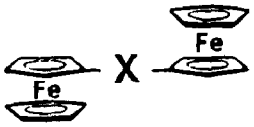

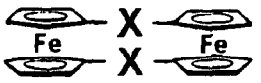

1 : X = CH_2

2 : X = CH_2CH_2

3 : X = $C(CH_3)_2$

4 : X = Hg

5 : X = C≡C

6 : X = $(C{\equiv}C)_2$

7 : X = CH_2

8 : X = $CH(CH_3)$

9 : X = $Sn(n\text{-}C_4H_9)_2$

10 : X = $SnI(n\text{-}C_4H_9)$

11 : X = C=C

[6,7] and **8** [8] are examples of such "localized" mixed-valence bridged biferrocenes. The second type of mixed-valence bridged biferrocene is completely delocalized on all spectroscopic time scales. Monooxidized cations of compounds **11** [6,7] and **12** [7,9] exemplify this second type.

When mixed-valence compounds are studied in solution, the energy and band shape of the intervalence transfer (IT) electronic absorption band, generally seen in the near-IR region, characterize the degree of delocalization and the rate of thermal electron transfer [1]. The simple Hush model [10] or Piepho–Krausz–Schatz (PKS) vibronic model [11] can be used to analyze the IT band. It has generally been accepted that the extent of metal–metal interaction in the σ-bridged mixed-valence system takes place through a space mechanism, and in π-bridged systems, through a bond mechanism with through-space interactions contributing once the metal centers are close enough to allow direct metal–metal interaction [12]. We report here the studies of a mixed-valence dibridged compound, **9**, in order to see what effect the bridged group has on the intramolecular electron transfer. We also report the first σ-dibridged mixed-valence compound which has an IT band in the near-IR region and suggest that the interaction involves a through-space mechanism, and perhaps through the bridge.

Experimental

Preparation of compounds

Solvents were routinely dried by standard procedures and stored under nitrogen. Compound **9** was prepared by a previously published procedure [13].

Oxidation of compound **9** by iodine in CH_2Cl_2 solution cleaves the Sn–C bond. In our hands, attempts to prepare an I_3^- salt of the mixed-valence monocation of compound **9** by use of stoichiometric amounts of iodine resulted in a mixture of orange and black materials upon evaporation. This orange material was obtained

and purified by chromatography on neutral activity II alumina. The first band, eluted with hexane, was compound **10** as identified by NMR. ^{1}H NMR ($CDCl_3$, δ): 0.7–1.6 (m, 18H, C_4H_9, with ^{117,119}Sn satellites), 4.16 (t, 8H, Cp), and 4.39 (t, 8H, Cp). Electron-impact mass spectrum, M^+ at m/e 974. Oxidation of compound **9** by iodine in benzene or hexane solution by a procedure similar to that used for biferrocene [8] gives the dioxidized triiodide salt as characterized by Mössbauer spectroscopy. Similar Sn–C bond cleavage was observed for the dioxidized triiodide salt in organic solvents, such as CH_2Cl_2. We also found that compound **9** is dioxidized by *p*-benzoquinone and HBF_4 in ether to give a BF_4^- salt which is quite stable in CH_2Cl_2 for several days. Anal. Found: C, 42.41; H, 4.88. $C_{36}H_{52}Fe_2Sn_2 \cdot 2BF_4$ calcd.: C, 42.92; H, 5.20%. Oxidation of compound **10** by *p*-benzoquinone/HBF_4 or *p*-benzoquinone/HPF_6 in ether solution by a procedure similar to that used for compound **9** gives an unknown product as detected by elemental analysis.

Physical measurements. ^{1}H NMR spectra were recorded with a Bruker MSL 200 spectrometer. Mass spectra were recorded with a VG system, Model 70-250S.

Polarographic measurements were carried out with a Princeton Applied Research Model 173 polarograph. Cyclic voltammetry was performed with a stationary Pt electrode, which was cleaned after each run. Runs were duplicated for each sample. The measurements were carried out on 1×10^{-3} *M* CH_2Cl_2 solutions containing 0.1 *M* $(n\text{-}C_4H_9)_4NBF_4$ as supporting electrolyte. Degassing with nitrogen prefaced each run. The potentials quoted in this work are relative to a saturated aqueous calomel electrode at 25 °C.

Near-IR spectra were obtained with a Perkin–Elmer Lambda 9 spectrophotometer. The near-IR spectra were recorded from 2300 nm to 900 nm in CD_2Cl_2 in 1.0 cm quartz cells. The mixed-valence solution for **9** was generated by mixing equal concentrations of neutral and dioxidized complexes. Quantitative calculation based on the concentration of mixed-valence complex was corrected from the comproportionation constant.

Crystal structure determination of ***10****.* Orange needle crystal (0.25 × 0.17 × 0.19 mm), which had been grown by slow evaporation of a hexane solution, was used for data collection at room temperature. The cell dimensions and the space group data were obtained by standard methods with an Enraf–Nonius CAD-4 diffractometer. The θ–2θ scan technique was used to record the intensities of all the nonequivalent reflections for which $1 < 2\theta < 49.8°$. Absorption corrections were made. Of the

Table 1

Crystallographic data for **10**

Chemical formula: $C_{28}H_{34}Fe_2I_2Sn_2$	fw: 973.502
Crystal system: monoclinic	space group: $P2_1/c$
a 10.3282(14) Å	*T* 25 °C
b 10.7916(12) Å	λ 0.70930 Å
c 13.6772(18) Å	ρ_{calcd} 2.126 g cm^{-3}
β 94.080(12)°	*μ* 4.59 mm^{-1}
V 1520.57 Å^3	R_F [a] = 0.036
Z = 2	R_{WF} [a] = 0.031
Transmission factor limits: 0.76108 to 0.99890	

[a] $R_F = \Sigma||F_o| - |F_c||/\Sigma F_o$; $R_{WF} = [\Sigma w(F_o - |F_c|)^2/\Sigma w F_o^2]^{1/2}$.

Table 2

Atom coordinates and thermal parameters for **10**

Atom	x	y	z	U_{iso}, [a] Å^2
I	0.37317(5)	0.05443(4)	0.13390(3)	5.44(2)
Sn	0.43167(3)	0.07925(3)	0.33061(2)	3.22(1)
Fe	0.26111(7)	−0.10285(6)	0.51814(5)	3.15(3)
C1	0.3280(5)	−0.0721(4)	0.3822(4)	3.4(2)
C2	0.3796(5)	−0.1860(5)	0.4241(4)	3.6(2)
C3	0.2761(6)	−0.2655(5)	0.4427(4)	4.4(3)
C4	0.1591(6)	−0.2040(5)	0.4121(4)	4.5(2)
C5	0.1907(5)	−0.0858(5)	0.3750(4)	4.0(2)
C6	0.6337(5)	0.0573(5)	0.3534(4)	3.6(2)
C7	0.7033(5)	−0.0488(5)	0.3939(4)	3.8(2)
C8	0.1624(5)	0.0199(5)	0.5988(4)	4.5(3)
C9	0.1468(6)	−0.1014(6)	0.6335(4)	4.7(3)
C10	0.7296(5)	0.1486(5)	0.3369(4)	4.0(2)
C11	0.3612(5)	0.2621(5)	0.3596(4)	3.9(2)
C12	0.2139(6)	0.2729(5)	0.3545(4)	5.0(3)
C13	0.1712(6)	0.4044(5)	0.3697(5)	5.1(3)
C14	0.0275(8)	0.4226(7)	0.3670(6)	7.5(4)
H2	0.476	−0.196	0.435	3.5(15)
H3	0.278	−0.348	0.476	10.2
H4	0.071	−0.240	0.419	4.3
H5	0.127	−0.019	0.355	8.3
H7	0.669	−0.131	0.414	7.2
H8	0.091	0.070	0.566	11.7
H9	0.061	−0.145	0.631	6.9
H10	0.702	0.230	0.308	2.9
H11A	0.411	0.288	0.303	3.6
H11B	0.396	0.276	0.429	4.5
H12A	0.203	0.246	0.284	5.9
H12B	0.174	0.251	0.416	7.5
H13A	0.209	0.450	0.429	8.0
H13B	0.217	0.466	0.330	8.1
H14A	0.014	0.514	0.374	13.3
H14B	−0.019	0.380	0.310	11.0
H14C	−0.009	0.374	0.422	9.4

[a] U_{iso} is the equivalent isotropic U defined as one-third of the trace of the orthogonalized U_{ij} tensor.

2833 independent intensities, 2161 with $F_o > 2.5\sigma(F_o^2)$ where $\sigma(F_o^2)$, were considered observed and were used in the final refinement. The crystal data are summarized in Table 1.

A three-dimensional Patterson synthesis was used to determine heavy-atom positions, which phased the data sufficiently well to permit location of the remaining non-hydrogen atoms from Fourier synthesis. All nonhydrogens were refined anisotropically. During the final cycles of refinement fixed hydrogen contributions with C–H bond lengths fixed at 1.08 Å were applied. The final positional parameters for all atoms are listed in Table 2, and the selected bond distances and angles are given in Table 3.

Supplementary material. Tables of anisotropic thermal parameters (Table s1, 1 page) and observed and calculated structure factors (Table s2, 19 pages) are available from the authors.

Table 3

Selected bond distances and angles for **10**

I–Sn	2.7283(6)	C(1)–C(2)	1.442(7)
Sn–C(1)	2.103(5)	C(1)–C(5)	1.422(7)
Sn–C(6)	2.102(5)	C(2)–C(3)	1.408(8)
Sn–C(11)	2.149(5)	C(3)–C(4)	1.415(8)
Fe–C(1)	2.055(5)	C(4)–C(5)	1.419(8)
Fe–C(2)	2.044(5)	C(6)–C(7)	1.441(7)
Fe–C(3)	2.048(5)	C(6)–C(10)	1.426(7)
Fe–C(4)	2.046(5)	C(7)–C(8)	1.418(8)
Fe–C(5)	2.048(5)	C(8)–C(9)	1.406(9)
Fe–C(6)	2.058(5)	C(9)–C(10)	1.408(8)
Fe–C(7)	2.049(5)	C(11)–C(12)	1.522(8)
Fe–C(8)	2.042(5)	C(12)–C(13)	1.504(8)
Fe–C(9)	2.037(5)	C(13)–C(14)	1.495(10)
Fe–C(10)	2.039(5)		
I–Sn–C(1)	99.94(13)	C(1)–C(2)–C(3)	109.1(5)
I–Sn–C(6)	106.46(13)	C(2)–C(3)–C(4)	107.7(5)
I–Sn–C(11)	102.57(13)	C(3)–C(4)–C(5)	108.3(5)
C(1)–Sn–C(6)	112.75(19)	C(1)–C(5)–C(4)	108.8(5)
C(1)–Sn–C(11)	117.62(20)	C(2)–C(1)–C(5)	106.1(4)
C(6)–Sn–C(11)	114.97(20)	C(6)–C(7)–C(8)	108.1(5)
Sn–C(6)–C(7)	127.5(4)	C(7)–C(8)–C(9)	108.4(5)
Sn–C(6)–C(10)	126.2(4)	C(8)–C(9)–C(10)	108.1(5)
Sn–C(1)–C(2)	127.8(4)	C(6)–C(10)–C(9)	109.2(5)
Sn–C(1)–C(5)	125.9(4)	C(7)–C(6)–C(10)	106.1(4)

Results and discussion

*Molecular structure of endo,endo-1,12-di-n-butyl-exo,exo-1,12-diiodo[1,1]stannaferrocenophane (**10**).* As shown in Fig. 1, the two metallocene moieties are linked to each other through tetrahedrally coordinated tin atoms. The molecule itself possesses a center of inversion. The average Sn–C bond length and bond angle for the bridged tin atoms are 2.12 Å and 105.43°, respectively. These values probably indicate sp^3 hybridized tin atoms. As can be clearly seen from Fig. 1, the results of the analysis confirm the *endo*-butyl configuration. [1,1]Stannaferrocenophanes are flexible and, if the substituents allow, can interconvert between two *anti*-oriented conformations. In the case of **10**, interconversion should take place from the *endo,endo*-dibutyl form to the sterically possible *exo,exo*-dibutyl form. The structural determination confirms that only the *endo,endo*-dibutyl isomer exists.

All of the iron–carbon bond distances in the ferrocene moieties are equal within experimental error. The average Fe–C bond distance (2.047(5) Å) is closer to the value of 2.045 Å found for ferrocene [14] than to the value of 2.075 Å found for the ferrocenium cation [15]. The dihedral angle between the two five-member rings of each ferrocene moiety is 3.38°; furthermore the two rings are nearly eclipsed with an average staggering angle of 6.5(4)°. The Cp rings are perfectly planar as indicated by the χ^2 values (Table 4) and distances to the plane from the ring atoms in the plane confirm this. The average C–C bond length (1.4205(7) Å) in the rings compares well with that in ferrocene (1.42 Å) [14]. The distance between the centers of mass of the two rings in each ferrocene moiety is 3.306 Å.

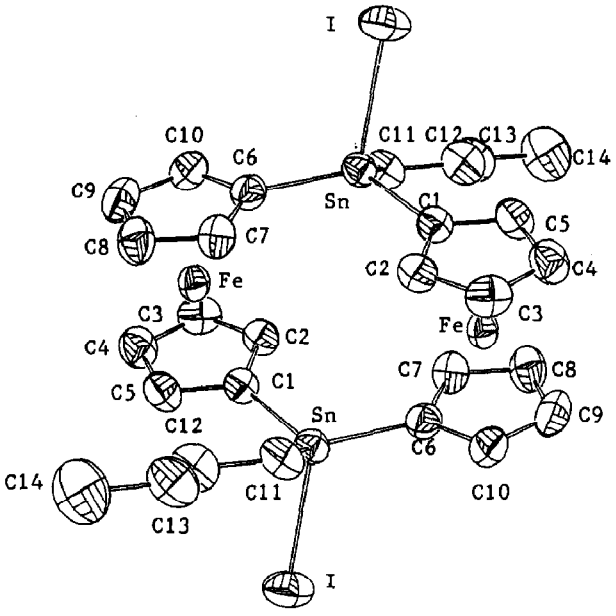

Fig. 1. ORTEP plot of **10** with 50% probability ellipsoids.

The distance between two iron atoms in a σ-dibridged mixed-valence compound is critical to a detailed understanding of the rate of intramolecular electron transfer. It has been generally accepted that the near-IR transition in the σ-bridged derivatives is attributed to a through-space mechanism [12]. If this suggestion is correct, then the distance between two iron atoms in a σ-bridged mixed-valence compound will be the only factor in controlling the intramolecular electron transfer. The Fe–Fe distance in compound **10** is listed in Table 5, as well as those for some other relevant σ-bridged mixed-valence compounds. The effect of Fe–Fe distance on intramolecular electron transfer will be discussed in more detail in the next section.

Electrochemical results. The neutral compound **9** undergoes two successive reversible one-electron oxidations to yield the mono- and then the dication. Electrochemical reversibility was demonstrated by the peak-to-peak separation between the

Table 4

Least squares planes and distances to the plan from the ring atoms

(a) C1–C5 ring			
$1.04(3)x + 4.21y + 12.582(16)z = 4.159(14)$			
C1	0.003(6)	C2	−0.004(7)
C3	0.003(8)	C4	0.000(7)
C5	−0.002(7)		
	$\chi^2 = 0.785$		
(b) C6–C10 ring			
$-1.55(3)x + 3.87(3)y + 12.717(15)z = 7.437(14)$			
C6	0.002(7)	C7	−0.002(7)
C8	0.002(7)	C9	−0.001(8)
C10	0.001(7)		
	$\chi^2 = 0.331$		

Table 5

Comparison of the Fe–Fe distances for **10** with other relevant compounds

Compound	Fe–Fe (Å)
8 [a]	4.6
9 [b]	5.50
10	5.47

[a] From ref. 16. [b] From ref. 13.

resolved reduction and oxidation wave maxima. The half-wave potentials for **9**, as well as those for some other relevant bridged compounds, are given in Table 6.

In the bridged biferrocenes there are two possible types of interaction between the two ferrocene moieties: (i) interaction propagated through the bridge and (ii) through space (electric field effect). In the case of σ-bridged biferrocenes, it has generally been accepted that the extent of metal–metal interaction is attributed to a through-space mechanism [12]. Furthermore, it has been shown that the magnitude of the peak-to-peak separation ($\Delta E_{1/2}$) gives an indication of the interaction between the two Fe sites [18]. Therefore, the magnitude of $\Delta E_{1/2}$ decreases as the Fe–Fe distance in a σ-bridged biferrocene increases. A comparison of the magnitude of $\Delta E_{1/2}$ of **9** (0.20 V) with that of **8** (0.19 V) indicates that the magnitude of interaction between the two Fe sites in **9** is similar to that in **8**, although the Fe–Fe distance in **9** (5.50 Å) is longer than that in **8** (4.6 Å). Although a through-space mechanism cannot be excluded, we speculate that the d–π overlap of tin atoms and the cyclopentadiene rings in **9** plays an important role.

Coulometry experiments show that each of the two waves is a one-electron-transfer process. In eq. 1 the abbreviation **3,3** is for the dioxidized salt, **2,3** for the monooxidized salts,

$$\mathbf{3,3} + \mathbf{2,2} \overset{K}{\rightleftharpoons} 2\,\mathbf{2,3} \qquad (1)$$

and **2,2** for the neutral compound. K for this comproportionation constant equi-

Table 6

Polarographic data for various bridged biferrocenes

compound	$E_{1/2}$	$\Delta E_{1/2}$, [a] V
Ferrocene	0.38	
1 [b]	0.30	0.1
	0.40	
2 [c]	0.37	0.0
3 [b]	0.28	0.16
	0.44	
4 [c]	0.28	0.08
	0.36	
7 [b]	0.25	0.19
	0.44	
8 [b]	0.23	0.20
	0.43	
9	0.50	0.20
	0.70	

[a] Peak separation between two waves. [b] In 90% EtOH aq. vs. SCE (from ref. 17). [c] From ref. 18.

librium is 2.45×10^3, as calculated from $E_{1/2}$ values at 25 °C. Quantitative calculations based on **2,3**, which appear in next section, have been corrected for the equilibrium.

Near-infrared spectra. The mixed-valence cation of **9** has a near-IR transition at 1700 nm, which is not present for the neutral complex or dioxidized ion. The band is very weak ($\epsilon = 8.4\ M^{-1}\ cm^{-1}$ in CD_2Cl_2 and is 3% broader than that estimated from the basis of the equation given by Hush [10] ($\Delta\nu_{1/2} = 3788\ cm^{-1}$ compared with a calculated value of 3678 cm^{-1}). Agreement to within about 10% That the $\Delta\nu_{1/2cal}$ and the $\Delta\nu_{1/2obs}$ values is usually taken as an indication that Hush model is a satisfactory description of a mixed-valence system. The intensity of the IT band is dependent on the degree of interaction of the donor and acceptor sites in the ground state. The values of the interaction parameter (α) and the electron transfer rate constant (K_{et}) can be estimated from eqs. 2 and 3, respectively.

$$\alpha^2 = \left\{(4.24 \times 10^{-4})\ \Delta\nu_{1/2}\epsilon_{max}\right\}/(\bar{\nu}r^2) \tag{2}$$

$$K_{et} = (2\pi/\hbar)V_{ab}{}^2(\pi/K_B T\bar{\nu})^{1/2}\ \exp(-\bar{\nu}/4K_B T) \tag{3}$$

$$V_{ab} = \left\{\left(4.24 \times 10^{-4}\epsilon_{max}\ \Delta\nu_{1/2}\bar{\nu}\right)/r^2\right\}^{1/2} \tag{4}$$

In eqs. 2, 3, and 4 the ϵ_{max} is extinction coefficient, r is the donor–acceptor distance, α is the mixing coefficient, $\Delta\nu_{1/2}$ is the bandwidth, and $\bar{\nu}$ is the frequency. The Fe–Fe distance (5.50 Å) in **9** is used as donor–acceptor distance. Thus $\alpha = 0.0087$ and $K_{et} = 6.66 \times 10^8$. Under the classification defined by Robin and Day [19], the cation of **9** is a class II mixed-valence compound.

The presence of the IT band in the mixed-valence cation of **9** while being absent in the cations of **7** and **8** is intriguing. It has been reported that the near-IR transition in the π-bond bridged derivatives is attributed to a predominantly through-bond mechanism whereas the transition in the σ-bridged derivatives is attributed to a through-space mechanism [12]. If the intramolecular electron transfer in **9** is attributed to a through-space mechanism, then there cannot be an IT band in the near-IR region. We believe that the Fe–Fe distance in the cation of **9** is longer than that in the cation of **8**. The Fe–Fe distances in the neutral **8** and **9** are listed in Table 5. A through-space mechanism cannot be excluded, but we propose that the presence of the IT band for the cation of **9** and its absence for the cation of **8** is due to a difference in the d–π overlap of tin atoms and the cyclopentadiene rings in the two systems. To our knowledge, this is a first rigid σ-dibridged mixed-valence compound which shows an IT band. All of the cations of ferricenyl(III)tris(ferrocenyl(II)) borate, triferrocenylmethane and diferrocenylphenylphosphine oxide, which are flexible σ-monobridged mixed-valence derivatives, exhibit the intervalence transition band [12]. Furthermore, the d–π overlap of bridged atom and Cp ring was speculated for diferrocenylphenylphosphine oxide cation [12].

Acknowledgement

We are grateful for support from the ROC National Science Council.

References

1 (a) P. Day, Int. Rev. Phys. Chem., 1 (1981) 149. (b)D.B. Brown, (Ed.) in Mixed-Valence Compounds, Theory and Applications in Chemistry, Physics, Geology and Biology, Reidel, Boston, MA, 1980.

2 M.J. Cohn, T.-Y. Dong, D.N. Hendrickson, S.J. Geib, and A.L. Rheingold, J. Chem. Soc., Chem. Commun., (1985) 1095
3 T.-Y. Dong, D.N. Hendrickson, K. Iwai, M.J. Cohn, S.J. Geib, A.L. Rheingold, H. Sano. I. Motoyama, and S. Nakashima, J. Am. Chem. Soc., 107 (1985) 7996.
4 S. Iijima, R. Saida, I. Motoyama, and H. Sano, Bull. Chem. Soc. Jpn., 54 (1981) 1375.
5 M. Konno, S. Hyodo, and S. Iijima, Bull. Chem. Soc. Jpn., 55 (1982) 2327.
6 I. Motoyama, M. Watanabe, and H. Sano, Chem. Lett., (1978) 513.
7 J.K. Kramer and D.N. Hendrickson, Inorg. Chem., 19 (1980) 3330.
8 (a) M.F. Moore, S.R. Wilson, M.J. Cohn, T.-Y. Dong, U.T. Mueller-Westerhoff, and D.N. Hendrickson, Inorg. Chem., 24 (1985) 4559. (b) W.H. Jr. Morrison and D.N. Hendrickson, Inorg. Chem., 14 (1975) 2331.
9 M. Hillman and A. Kvick, Organometallics, 2 (1983) 1780.
10 N.S. Hush, Prog. Inorg. Chem., 8 (1967) 391.
11 K.Y. Wong and P.N. Schatz, Prog. Inorg. Chem., 28 (1981) 369 and references therein.
12 F. Delgado-Pena, D.R. Talham, and D.O. Cowan, J. Organomet. Chem., 253 (1983) C43.
13 A. Clearfield and C.J. Simmons, Inorg. Chim. Acta, 75 (1983) 139.
14 P. Seiler and J.D. Dunitz, Acta Crystallogr., Sect B, 35 (1979) 1068.
15 N.J. Mammano, A. Zalkin, A. Landers, and A.L. Rheingold, Inorg. Chem., 16 (1977) 297.
16 J.S. McKechnie, C.A. Maier, B. Bersted, and I.C. Paul, J. Chem. Soc., Perkin Trans. II, (1973) 138.
17 J.E. Gorton, H.L. Lentzner, and W.E. Watts, Tetrahedron, 27 (1971) 4353.
18 W.H.Jr. Morrison, S. Krogsrud, and D.N. Hendrickson, Inorg. Chem., 12 (1973) 1998.
19 M.B. Robin and P. Day, Advan. Inorg. Chem. Radiochem., 10 (1967) 247.